RESEARCH ARTICLE | FEBRUARY 16 2024

Solving the time-dependent protein distributions for autoregulated bursty gene expression using spectral decomposition

Bingjie Wu; James Holehouse; Ramon Grima ; Chen Jia

J. Chem. Phys. 160, 074105 (2024)
https://doi.org/10.1063/5.0188455

The Journal of Chemical Physics ARTICLE pubs.aip.org/aip/jcp

Solving the time-dependent protein distributions for autoregulated bursty gene expression using spectral decomposition

Cite as: J. Chem. Phys. 160, 074105 (2024); doi: 10.1063/5.0188455
Submitted: 21 November 2023 • Accepted: 19 January 2024 •
Published Online: 16 February 2024

Bingjie Wu,[1] James Holehouse,[2] Ramon Grima,[3,a)] and Chen Jia[1,a)]

AFFILIATIONS

[1] Applied and Computational Mathematics Division, Beijing Computational Science Research Center, Beijing 100193, China
[2] The Santa Fe Institute, 1399 Hyde Park Rd., Santa Fe, New Mexico 87501, USA
[3] School of Biological Sciences, University of Edinburgh, Edinburgh EH9 3BF, United Kingdom

[a)] **Authors to whom correspondence should be addressed:** ramon.grima@ed.ac.uk and chenjia@csrc.ac.cn

ABSTRACT

In this study, we obtain an exact time-dependent solution of the chemical master equation (CME) of an extension of the two-state telegraph model describing bursty or non-bursty protein expression in the presence of positive or negative autoregulation. Using the method of spectral decomposition, we show that the eigenfunctions of the generating function solution of the CME are Heun functions, while the eigenvalues can be determined by solving a continued fraction equation. Our solution generalizes and corrects a previous time-dependent solution for the CME of a gene circuit describing non-bursty protein expression in the presence of negative autoregulation [Ramos *et al.*, Phys. Rev. E **83**, 062902 (2011)]. In particular, we clarify that the eigenvalues are generally not real as previously claimed. We also investigate the relationship between different types of dynamic behavior and the type of feedback, the protein burst size, and the gene switching rate.

I. INTRODUCTION

It is well known that often the expression of a gene is related to that of other genes. These gene–gene interactions are at the heart of gene regulatory networks.[1] Perhaps the simplest type of such interactions is autoregulation, whereby a protein influences its own transcription, leading to positive or negative feedback. This type of regulation is common, e.g., it is estimated that about 40% of *Escherichia coli*'s transcription factors self-regulate, mostly engaging in autorepression.[2,3]

Over the past 20 years, many stochastic models of autoregulation have been developed and their steady-state behavior has been studied using both simulations and theory. Within the continuous-time Markovian framework, some of these studies make headway by modelling gene state changes implicitly and assuming that protein numbers are real and positive (a continuum assumption).[4–8] Other studies have tackled the more realistic problem where the changes in molecule numbers of both gene and protein, when reactions occur, are integers.[9–12] Of the latter class of models, some assume that protein expression occurs one at a time,[9,10] while others assume that expression occurs in stochastic bursts.[11,12] Another distinguishing feature is that some models assume that there is no change in the protein number when a protein copy binds to a gene or when it unbinds,[9,11] while others model the change explicitly.[10,12] We note that the majority of these stochastic models have been solved exactly only in steady-state conditions. The exact time-dependent solution, being a much harder mathematical problem, has received considerably less attention—in Ref. 13, a model of non-bursty protein expression, including negative autoregulation, was purportedly solved exactly. A recent review of the various types of stochastic models of autoregulatory genetic circuits that also compares and contrasts their predictions can be found in Ref. 14.

In the present paper, we construct and exactly solve in time a stochastic model of bursty or non-bursty protein expression in the presence of positive or negative autoregulation, where both gene and protein numbers are modelled discretely. In Sec. II, the reac-

tion scheme and the chemical master equation (CME) describing the stochastic dynamics of the set of reactions are introduced. In Sec. III, by means of the method of spectral decomposition, we show that the eigenfunctions of the time-dependent generating function solution of the CME are Heun functions, while the eigenvalues obey a continued fraction equation that is obtained by considering the holomorphism of the generating function. The accuracy of the solution is verified by stochastic simulations. Crucially, we also show that a previous time-dependent solution for the CME of a gene circuit describing non-bursty protein expression in the presence of negative autoregulation[13] is incorrect because the eigenvalues are generally not real as previously claimed. In Sec. IV, we investigate the relationship between five different types of dynamic behavior and the type of feedback, the protein burst size, and the gene switching rate. We conclude with a discussion in Sec. V.

II. MODEL

Here, we consider stochastic gene expression dynamics in a minimal coupled positive-plus-negative feedback loop with gene state switching, protein synthesis, and protein decay (Fig. 1). Let G and G^* denote the inactive and active states of the gene, and let P denote the corresponding protein. In the active state G^*, we assume that the protein is produced in a non-bursty (constitutive) or bursty manner. Both non-bursty and bursty gene expression are commonly observed in naturally occurring systems. Bursty protein synthesis is often due to rapid translation of protein from a single, short-lived mRNA molecule;[15,16] if the mRNA lifetime is quite long (as common in mammalian cells[17]), then protein synthesis may appear non-bursty.

Let n be the copy number of the protein. In the bursty case, the reaction scheme underlying the coupled feedback loop is as follows [Fig. 1(a)]:

$$G \xrightarrow{a+\mu n} G^*, \quad G^* \xrightarrow{b+\nu n} G,$$
$$G^* \xrightarrow{\rho p^k (1-p)} G^* + kP, \quad k \geq 1, \quad P \xrightarrow{d} \varnothing. \tag{1}$$

Due to feedback regulation, the protein number n will directly or indirectly affect the switching rates between the two gene states. Here, a and b are the spontaneous switching rates, μ and ν characterize the strengths of positive and negative feedback loops, respectively, and d is the decay rate of the protein either due to protein degradation or due to dilution during cell division.[18] Specifically, the protein decay rate can be represented as $d = \log 2/T_p + \log 2/T_c$, where T_p is the protein half-life and T_c is the cell cycle time. When the gene is in the active state G^*, the synthesis of the protein occurs in bursts with frequency ρ and random size k sampled from a geometric distribution with parameter p, in agreement with experiments.[19] Note that the model considered here is more general than the classical model of autoregulatory feedback loops proposed by Kumar *et al.*[11] In particular, the model describes a positive autoregulatory loop if the negative feedback strength ν vanishes, and it describes a negative autoregulatory loop if the positive feedback strength μ vanishes. In a coupled feedback loop, both μ and ν are nonzero. Coupled gene circuits widely exist in nature, and they have been shown to be a crucial network motif to produce robust and tunable biological oscillations.[20] Biological examples of coupled feedback loops can be found in Refs. 20 and 21.

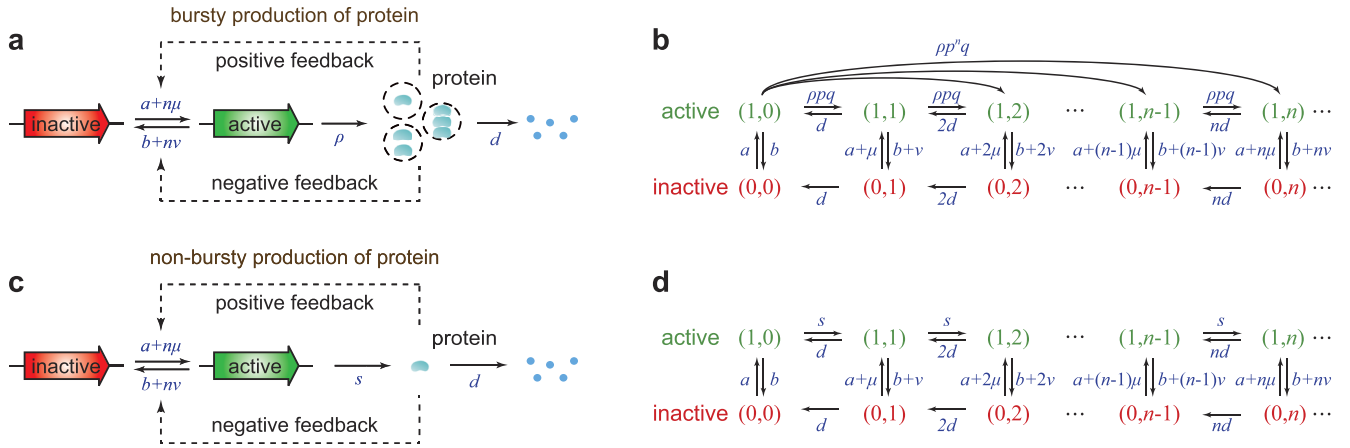

FIG. 1. Models. (a) A minimal coupled gene circuit with positive-plus-negative feedback. When the gene is active, the protein is produced in a bursty manner with the burst size having a geometric distribution. (b) Transition diagram of the Markovian dynamics for the model illustrated in (a). Note that translational bursting can cause jumps from any microstate $(1, n)$ to $(1, n + k)$ [this is only shown for microstate (1, 0) in the figure but is also true for any other microstate $(1, n)$]. (c) Same as (a) except that the protein is produced in a non-bursty manner when the gene is active, i.e., protein molecules are produced one at a time. (d) Transition diagram of the Markovian dynamics for the model illustrated in (c).

The microstate of the gene can be represented by an ordered pair (i,n), where i is the gene state with $i=0,1$ corresponding to the inactive and active states, respectively, and n is the protein number. Let $p_{i,n}(t)$ denote the probability of having n protein molecules in an individual cell when the gene is in state i. Then, the stochastic gene expression dynamics can be described by the Markov jump process shown in Fig. 1(b). The evolution of the Markovian dynamics is governed by the CMEs,

$$\begin{cases} \dot{p}_{0,n} = d[(n+1)p_{0,n+1} - np_{0,n}] + [(b+\nu n)p_{1,n} - (a+\mu n)p_{0,n}], \\ \dot{p}_{1,n} = \rho\left[\sum_{k=0}^{n-1} p^{n-k}(1-p)p_{1,k} - pp_{1,n}\right] + d[(n+1)p_{1,n+1} - np_{1,n}] + [(a+\mu n)p_{0,n} - (b+\nu n)p_{1,n}], \end{cases} \tag{2}$$

where the term involving ρ on the right-hand side represents protein synthesis, the terms involving d represent protein decay, and the terms involving a, b, μ, and ν represent gene state switching and feedback control.

In the non-bursty case, the reactions describing the coupled feedback loop are as follows [Fig. 1(c)]:

$$G \xrightarrow{a+\mu n} G^*, \quad G^* \xrightarrow{b+\nu n} G, \qquad G^* \xrightarrow{s} G^* + P, \quad P \xrightarrow{d} \varnothing. \tag{3}$$

Here, we assume that protein molecules are produced one at a time with rate s when the gene is active. The Markovian dynamics for this model is illustrated in Fig. 1(d). Note that the non-bursty model described by Eq. (3) is a limiting case of the bursty model described by Eq. (1).[22,23] Since the protein burst size is geometrically distributed, its expected value is given by $B = \sum_{k=1}^{\infty} kp^k(1-p) = p/(1-p)$. It is easy to see that when $\rho \to \infty$ and $B \to 0$, while keeping $\rho B = s$ as constant, we have $p \to 0$ and

$$\rho p(1-p) \to s, \quad \rho p^k(1-p) \to 0, \quad k \geq 2. \tag{4}$$

This shows that the bursty model reduces to the non-bursty one in the above limit. Hence, in the following, we will first derive analytical results for the bursty model and then use them to obtain relevant results for the non-bursty model by taking the above limit.

We emphasize that the exact time-dependent distributions for the non-bursty model have been discussed in Ref. 13 in the special case of negative autoregulation ($\mu = b = 0$). However, we find that the solution given in Ref. 13 is both mathematically inconsistent and incomplete (the detailed reasons will be explained later). Here, we generalize and correct the results obtained in previous studies by taking translational bursting and coupled feedback into account.

III. SOLVING THE TIME-DEPENDENT MASTER EQUATION

A. Time-dependent solution for the bursty model

We first compute the time-dependent distributions of protein numbers for the bursty model. To this end, we define a pair of generating functions,

$$f_i(t,z) = \sum_{n=0}^{\infty} p_{i,n}(t)z^n, \quad i = 0,1. \tag{5}$$

Moreover, let $p_n(t) = p_{0,n}(t) + p_{1,n}(t)$ denote the probability of having n protein molecules in an individual cell and let $f(t,z) = f_0(t,z) + f_1(t,z)$ denote its generating function. Then, Eq. (2) can be converted into the following set of partial differential equations (PDEs):

$$\begin{cases} \partial_t f_0 = d(1-z)\partial_z f_0 - af_0 - \mu z\partial_z f_0 + bf_1 + \nu z\partial_z f_1, \\ \partial_t f_1 = \dfrac{\rho p(z-1)}{1-pz} f_1 + d(1-z)\partial_z f_1 + af_0 + \mu z\partial_z f_0 - bf_1 - \nu z\partial_z f_1. \end{cases} \tag{6}$$

Following Ref. 13, we use the method of spectral decomposition to solve this set of PDEs. To this end, we assume that the generating functions f_i have the variable separation form of $f_i(t,z) = e^{\lambda t}\tilde{f}_i(z)$. Here, λ is called an *eigenvalue* of the PDEs given in Eq. (6) and $\tilde{f}_i(z)$, $i = 0, 1$, are called the corresponding *eigenfunctions*. Inserting it into Eq. (6) yields

$$\begin{cases} \lambda\tilde{f}_0 = d(1-z)\partial_z\tilde{f}_0 - a\tilde{f}_0 - \mu z\partial_z\tilde{f}_0 + b\tilde{f}_1 + \nu z\partial_z\tilde{f}_1, \\ \lambda\tilde{f}_1 = \dfrac{\rho p(z-1)}{1-pz}\tilde{f}_1 + d(1-z)\partial_z\tilde{f}_1 + a\tilde{f}_0 + \mu z\partial_z\tilde{f}_0 - b\tilde{f}_1 - \nu z\partial_z\tilde{f}_1. \end{cases} \tag{7}$$

Moreover, let $f(t,z) = e^{\lambda t}\tilde{f}(z)$ with $\tilde{f}(z) = \tilde{f}_0(z) + \tilde{f}_1(z)$. Adding the two identities in Eq. (7), we obtain

$$\tilde{f}_1 = \frac{1-pz}{\rho p(z-1)}\left[\lambda\tilde{f} - d(1-z)\partial_z\tilde{f}\right]. \tag{8}$$

It then follows that

$$\tilde{f}_0 = \tilde{f} - \tilde{f}_1 = \tilde{f} - \frac{1-pz}{\rho p(z-1)}\left[\lambda\tilde{f} - d(1-z)\partial_z\tilde{f}\right]. \tag{9}$$

Substituting Eqs. (8) and (9) into the second row of Eq. (7) and eliminating $\tilde{f}_0$ and $\tilde{f}_1$, we find that $\tilde{f}$ satisfies the following second-order ordinary differential equation (ODE):

$$d(z-1)^2(pz-1)[(\mu+\nu+d)z-d]\tilde{f}''(z) + (z-1)M_1(z)\tilde{f}'(z) + N_1(z)\tilde{f}(z) = 0, \tag{10}$$

where

$$M_1(z) = [(\mu+\nu+2d)\lambda + [d^2+(\mu+\nu+a+b+\rho)d+\mu\rho]]pz^2 - [(\mu+\nu+2d+2dp)\lambda + [2d^2+(\mu+\nu+a+b+2\rho)d + \mu\rho]p + (a+b)d]z + 2d\lambda + (d^2+\rho d)p + (a+b)d,$$

$$N_1(z) = [\lambda^2+(a+b+\rho)\lambda + a\rho]pz^2 - [(p+1)\lambda^2 - [(a+b+d + \mu+\nu+2\rho)p + (a+b-d-\mu-\nu)]\lambda - 2a\rho p]z + \lambda^2 + [(d+\rho)p + a + b - d]\lambda + a\rho p.$$

Note that the above ODE has four regular singularities 1, $1/p$, $d/(\mu+\nu+d)$, and ∞. The crucial idea is to transform it into a Heun differential equation.[13] In fact, the regular singularities of the standard Heun differential equation are 0, 1, ξ, and ∞ for some constant ξ (Ref. 24, Sec. 31.2). Thus, we need to make a variable transformation that maps $\{d/(\mu+\nu+d), 1, 1/p, \infty\}$ onto $\{0, 1, \xi, \infty\}$. To this end, we introduce a new variable

$$x = \frac{(\mu+\nu+d)z - d}{\mu+\nu}.$$

Moreover, let h be the function with the variable x associated with $\tilde{f}$, i.e.,

$$h(x) = \tilde{f}(z) = \tilde{f}\left(\frac{(\mu+\nu)x+d}{\mu+\nu+d}\right).$$

Then, Eq. (10) can be transformed into the second-order ODE,

$$x(x-1)^2(x-\xi)h''(x) + (x-1)M_2(x)h'(x) + N_2(x)h(x) = 0,$$

where $\xi = (\mu+\nu+d-dp)/[(\mu+\nu)p]$ is a constant and

$$M_2(x) = \frac{\mu+\nu+d}{(\mu+\nu)^2 dp} M_1\left(\frac{(\mu+\nu)x+d}{\mu+\nu+d}\right),$$
$$N_2(x) = \frac{\mu+\nu+d}{(\mu+\nu)^2 dp} N_1\left(\frac{(\mu+\nu)x+d}{\mu+\nu+d}\right)$$

are functions of x. To proceed, we define a new function $\tilde{h}(x) = (x-1)^{\lambda/d}h(x)$. It is easy to check that $\tilde{h}(x)$ satisfies the following standard Heun differential equation:

$$\tilde{h}''(x) + \left(\frac{\gamma}{x} + \frac{\delta}{x-1} + \frac{\epsilon}{x-\xi}\right)\tilde{h}'(x) + \frac{\alpha\beta x - q}{x(x-1)(x-\xi)}\tilde{h}(x) = 0, \tag{11}$$

where

$$\gamma = \frac{(\mu+\nu+d-dp)\lambda + (a+b+\rho p)\nu + (\mu+d-dp)(a+b)}{(\mu+\nu+d)(\mu+\nu+d-dp)},$$
$$\delta = -\frac{\lambda}{d}, \quad \epsilon = \frac{d^2(1-p) + (\mu+\nu+\rho-\rho p)d + \mu\rho}{d(\mu+\nu+d-dp)},$$
$$\alpha\beta = \frac{(ad-\lambda\mu)\rho}{d^2(\mu+\nu+d)}, \quad \alpha+\beta = \gamma+\delta+\epsilon-1, \quad q = \frac{(\mu+\nu)a\rho + \lambda\mu\rho}{d(\mu+\nu+d)(\mu+\nu)}. \tag{12}$$

It is a classical result[25,26] that the two general solutions of Eq. (11) are given by

$$(x-1)^{1-\delta}Hl(\xi, q_1; \alpha_1, \beta_1, \gamma, 2-\delta; x),$$
$$x^{1-\gamma}(x-1)^{1-\delta}Hl(\xi, q_2; \alpha_2, \beta_2, 2-\gamma, 2-\delta; x),$$

where Hl is the *local Heun function* (it is also referred to as the general Heun function[25]) and

$$q_1 = q - (\delta-1)\gamma\xi, \quad \alpha_1 = \alpha+1-\delta, \quad \beta_1 = \beta+1-\delta,$$
$$q_2 = q - (\gamma+\delta-2)\xi - (\gamma-1)\epsilon, \quad \alpha_2 = \alpha-\gamma-\delta+2, \quad \beta_2 = \beta-\gamma-\delta+2. \tag{13}$$

Hence, the two linearly independent solutions of Eq. (10) are given by

$$(z-1)Hl\left(\xi, q_1; \alpha_1, \beta_1, \gamma, 2-\delta; \frac{\mu+\nu+d}{\mu+\nu}(z-z_0)\right), \tag{14}$$

$$(z-z_0)^{1-\gamma}(z-1)Hl\left(\xi, q_2; \alpha_2, \beta_2, 2-\gamma, 2-\delta; \frac{\mu+\nu+d}{\mu+\nu}(z-z_0)\right), \tag{15}$$

where $z_0 = d/(\mu+\nu+d)$.

We next make a crucial observation that in our model, the protein distribution $p_n(t)$ must decay exponentially with respect to the protein number n when $n \geq 1$ (see Sec. 1 of the supplementary material for the proof). In other words, $p_n(t)$ must have the following approximation:

$$p_n(t) \sim K(t)e^{-\gamma n}, \quad n \geq 1, \tag{16}$$

where $K(t)$ is a constant depending on t and $\gamma > 0$ describes the decay rate of $p_n(t)$ with respect to n. This shows that

$$\limsup_{n\to\infty} \sqrt[n]{p_n(t)} \leq e^{-\gamma} < 1.$$

By the root test,[27] the convergence radius of the power series given in Eq. (5) must be greater than 1. Since $z_0 < 1$, the generating function $f(t,z)$, as well as the function $\tilde{f}(z)$, must be holomorphic at both $z = z_0$ and $z = 1$. Recall that $\tilde{f}(z)$ has two linearly independent solutions. In Sec. 2 of the supplementary material, we prove that the solution given in Eq. (15) cannot be holomorphic at both $z = z_0$ and $z = 1$. Hence, we only need to consider the other solution given in Eq. (14).

Since the local Heun function $Hl(\xi, q_1; \alpha_1, \beta_1, \gamma, 2-\delta; x)$ is holomorphic in the unit disk $|x| < 1$, it is clear that the solution given in Eq. (14) must be holomorphic at $z = z_0$. On the other hand, the solution given in Eq. (14) is holomorphic at $z = 1$ if and only if the function $Hl(\xi, q_1; \alpha_1, \beta_1, \gamma, 2-\delta; x)$ is holomorphic at $x = 1$. Note that the parameters q_1, α_1, β_1, γ, and δ are all functions of the eigenvalue λ [see Eqs. (12) and (13)]. It is an important property of the local Heun function (Ref. 24, Sec. 31.4) that $Hl(\xi, q_1; \alpha_1, \beta_1, \gamma, 2-\delta; x)$ is holomorphic at $x = 1$ if and only if λ satis-

fies the following continued fraction equation (also refer to Ref. 28):

$$q_1 = \frac{R_0^{(1)}P_1^{(1)}}{(Q_1^{(1)}+q_1)-}\frac{R_1^{(1)}P_2^{(1)}}{(Q_2^{(1)}+q_1)-}\frac{R_2^{(1)}P_3^{(1)}}{(Q_3^{(1)}+q_1)-}\cdots, \tag{17}$$

where

$$R_n^{(1)} = \xi(n+1)(n+\gamma), \quad P_n^{(1)} = (n-1+\alpha_1)(n-1+\beta_1),$$
$$Q_n^{(1)} = n[(n-1+\gamma)(1+\xi)+\xi(2-\delta)+\alpha_1+\beta_1-\gamma+\delta-1].$$

Here, we have used the standard notation for continued fractions (Ref. 24, Sec. 1.12), i.e.,

$$\frac{d_1}{e_1\pm}\frac{d_2}{e_2\pm}\frac{d_3}{e_3\pm}\cdots = \frac{d_1}{e_1\pm\frac{d_2}{e_2\pm\frac{d_3}{e_3\pm\cdots}}}.$$

Solving Eq. (17) gives an infinite set of discrete values λ_n, $n = 1, 2, \ldots$, and these values are actually all nonzero eigenvalues of Eq. (6). Recall that the local Heun function $Hl(\xi, q_1;\ \alpha_1, \beta_1, \gamma, 2-\delta;\ x)$ is called a *Heun function*, denoted by Hf, if it is holomorphic at $x = 1$ (Ref. 24, Sec. 31.4). Then, the eigenfunctions corresponding to all nonzero eigenvalues are given by

$$\tilde{f}^{\lambda_n}(z) = (z-1)Hf\left(\xi, q_1; \alpha_1, \beta_1, \gamma, 2-\delta; \frac{\mu+\nu+d}{\mu+\nu}(z-z_0)\right), \quad n \geq 1,$$

where q_1, α_1, β_1, γ, and δ are all functions of eigenvalue λ_n.

We emphasize that solving the continued fraction equation can only give all nonzero eigenvalues. This is because for the zero eigenvalue $\lambda_0 = 0$, it follows from Eq. (12) that $\delta = 0$ and $\alpha\beta x - q = a\rho(x-1)/[d(\mu+\nu+d)]$. In this case, the Heun differential equation given in Eq. (11) reduces to the hypergeometric differential equation,

$$\tilde{h}''(x) + \left(\frac{\gamma}{x} + \frac{\epsilon}{x-\xi}\right)\tilde{h}'(x) + \frac{a\rho}{x(x-\xi)}\tilde{h}(x) = 0.$$

Similarly, by solving this equation, we find that the eigenfunction corresponding to the zero eigenvalue is given by

$$\tilde{f}^{\lambda_0}(z) = {}_2F_1(a_1, b_1; c_1; w(z-z_0)),$$

where

$$z_0 = \frac{d}{\mu+\nu+d}, \quad w = \frac{p(\mu+\nu+d)}{\mu+\nu+d-dp},$$
$$c_1 = \frac{(a+b+\rho p)\nu + (\mu+d-dp)(a+b)}{(\mu+\nu+d)(\mu+\nu+d-dp)}, \tag{18}$$
$$a_1+b_1 = c_1 + \frac{(\rho-\rho p)d+\mu\rho}{d(\mu+\nu+d-dp)}, \quad a_1b_1 = \frac{a\rho}{d(\mu+\nu+d)}.$$

So far, we have derived the eigenfunctions corresponding to all eigenvalues. The eigenfunction corresponding to the zero eigenvalue is a hypergeometric function, and the eigenfunctions corresponding to the nonzero eigenvalues have the form of Heun functions. By the Perron–Frobeniüs theorem, when the system is ergodic, one eigenvalue must be zero and the other eigenvalues must have negative real parts. Hence, all eigenvalues can be arranged so that

$$0 = \lambda_0 > \mathrm{Re}\,\lambda_1 \geq \mathrm{Re}\,\lambda_2 \geq \cdots, \tag{19}$$

where $\mathrm{Re}(z)$ denotes the real part of z.

Note that Eq. (17) must have an infinite number of solutions (Ref. 24, Sec. 31.4). Roughly speaking, this is because a continued fraction equation can be viewed as a polynomial equation of degree infinity with respect to λ. To solve these solutions numerically, we need to truncate Eq. (17) at a large integer N, with N being the number of layers of the continued fraction equation. The truncated equation is actually a polynomial equation of degree $2N+2$, and thus, it must have $2N+2$ roots, denoted by $\lambda_1^N, \lambda_2^N, \ldots, \lambda_{2N+2}^N$. These $2N+2$ roots could be arranged so that

$$\mathrm{Re}\,\lambda_1^N \geq \mathrm{Re}\,\lambda_2^N \geq \cdots \geq \mathrm{Re}\,\lambda_{2N+2}^N.$$

As the truncation size N increases, λ_n^N rapidly converges to the true eigenvalue λ_n, and thus, we can use λ_n^N as an accurate approximation of λ_n when N is large. According to our simulations, for a fixed N, the first $N/2$ roots of the truncated polynomial equation are very close to the true eigenvalues (supplementary material, Table 1).

Recall that the stochastic dynamics of the coupled feedback loop is described by the Markov jump process illustrated in Fig. 1(b). In fact, all nonzero eigenvalues determined by solving Eq. (17) are exactly the same as the all nonzero eigenvalues of the generator matrix for the Markov jump process. Table I compares the first ten solutions of the continued fraction equation (truncated at $N = 20$ with N being the number of layers of the continued fraction equation) and the first ten nonzero eigenvalues of the generator

TABLE I. Comparison of the first ten nonzero eigenvalues computed using two different methods. All nonzero eigenvalues of the PDEs given in Eq. (6) are the solutions to the continued fraction equation given in Eq. (17). These eigenvalues are in excellent agreement with all nonzero eigenvalues of the generator matrix of the Markovian dynamics illustrated in Fig. 1(b). The parameters are chosen as $\rho = 10$, $B = 1$, $d = 1$, $\mu = 0.2$, $\nu = 0.3$, $a = 1$, and $b = 1.5$.

Eigenvalues	λ_1	λ_2	λ_3	λ_4	λ_5, λ_6	λ_7, λ_8	λ_9, λ_{10}
Continued fraction method	−0.89	−1.82	−2.81	−3.66	$-4.52 \pm 0.33\mathbf{i}$	$-5.76 \pm 0.50\mathbf{i}$	$-6.99 \pm 0.57\mathbf{i}$
Generator matrix method	−0.89	−1.82	−2.81	−3.66	$-4.52 \pm 0.33\mathbf{i}$	$-5.76 \pm 0.50\mathbf{i}$	$-7.00 \pm 0.55\mathbf{i}$

matrix (truncated at $N = 200$, with N being the maximum protein number). Clearly, they coincide with each other perfectly and some eigenvalues may be complex numbers since the system is far from equilibrium.

We emphasize that when the protein number is large, the eigenvalues obtained using the generator matrix method may not be accurate since we need to compute the eigenvalues of a very large sparse matrix, which may lead to numerical instability. However, the continued fraction method still works in this case. Moreover, due to the rapid convergence of λ_n^N to λ_n, the truncation size for the continued fraction method is much smaller than that for the generator matrix method.

Thus far, we have obtained all eigenvalues λ_n, $n \geq 0$, and the corresponding eigenfunctions $\tilde{f}^{\lambda_n}$ are given by

$$\begin{aligned}\tilde{f}^{\lambda_0}(z) &= {}_2F_1(a_1, b_1; c_1; w(z - z_0)),\\ \tilde{f}^{\lambda_n}(z) &= (z-1)Hf\left(\xi, q_1; \alpha_1, \beta_1, \gamma, 2-\delta; \frac{\mu+\nu+d}{\mu+\nu}(z-z_0)\right), \quad n \geq 1.\end{aligned} \tag{20}$$

It follows from Eq. (8) that $\tilde{f}_1^{\lambda_n}$ are given by

$$\tilde{f}_1^{\lambda_n}(z) = \frac{1-pz}{\rho p(z-1)}\left[\lambda_n \tilde{f}^{\lambda_n}(z) + d(z-1)\partial_z \tilde{f}^{\lambda_n}(z)\right], \quad n \geq 0. \tag{21}$$

In this way, we can also determine $\tilde{f}_0^{\lambda_n} = \tilde{f}^{\lambda_n} - \tilde{f}_1^{\lambda_n}$. Finally, using the method of spectral decomposition, the generating functions f_i and f have the following series form:

$$f_i(t,z) = \sum_{n=0}^{\infty} C_n e^{\lambda_n t} \tilde{f}_i^{\lambda_n}(z), \quad f(t,z) = \sum_{n=0}^{\infty} C_n e^{\lambda_n t} \tilde{f}^{\lambda_n}(z). \tag{22}$$

Then, the time-dependent distribution of protein numbers can be recovered by taking the derivatives of the generating function f at $z = 0$, i.e.,

$$p_n(t) = \frac{1}{n!}\frac{\partial^n}{\partial z^n} f(t,z)\Big|_{z=0}. \tag{23}$$

The remaining question is how to determine the coefficients C_n in Eq. (22) based on the initial conditions. To this end, it follows from Eq. (22) that for any complex numbers $z_0, z_1, \ldots, z_M$,

$$\begin{bmatrix} f_0(0,z_0) \\ \vdots \\ f_0(0,z_M) \\ f_1(0,z_0) \\ \vdots \\ f_1(0,z_M) \end{bmatrix} = \begin{bmatrix} \tilde{f}_0^{\lambda_0}(z_0) & \tilde{f}_0^{\lambda_1}(z_0) & \cdots \\ \vdots & \vdots & \\ \tilde{f}_0^{\lambda_0}(z_M) & \tilde{f}_0^{\lambda_1}(z_M) & \cdots \\ \tilde{f}_1^{\lambda_0}(z_0) & \tilde{f}_1^{\lambda_1}(z_0) & \cdots \\ \vdots & \vdots & \\ \tilde{f}_1^{\lambda_0}(z_M) & \tilde{f}_1^{\lambda_1}(z_M) & \cdots \end{bmatrix} \begin{bmatrix} C_0 \\ C_1 \\ \vdots \end{bmatrix},$$

where $\tilde{f}_i^{\lambda_n}(z)$, $i = 0, 1$, are determined by Eqs. (20) and (21) and $f_i(0,z) = \sum_{n=0}^{\infty} p_{i,n}(0) z^n$, $i = 0, 1$, are determined by the initial conditions. Note that this is an infinite dimensional system of linear equations with variables C_n. In order to compute C_n, we need to truncate the system at a large integer M. To do this, we use an approach similar to the inverse discrete Fourier transform. Let M be a positive integer, and let $z_m = e^{2\pi m \mathbf{i}/M}$, $0 \leq m \leq M-1$, be all Mth roots of unity. Clearly, when $M \gg 1$, the coefficients C_n approximately satisfy the following set of linear equations:

$$\begin{bmatrix} f_0(0,z_0) \\ \vdots \\ f_0(0,z_{M-1}) \\ f_1(0,z_0) \\ \vdots \\ f_1(0,z_{M-1}) \end{bmatrix} = \begin{bmatrix} \tilde{f}_0^{\lambda_0}(z_0) & \tilde{f}_0^{\lambda_1}(z_0) & \cdots & \tilde{f}_0^{\lambda_{2M-1}}(z_0) \\ \vdots & \vdots & & \vdots \\ \tilde{f}_0^{\lambda_0}(z_{M-1}) & \tilde{f}_0^{\lambda_1}(z_{M-1}) & \cdots & \tilde{f}_0^{\lambda_{2M-1}}(z_{M-1}) \\ \tilde{f}_1^{\lambda_0}(z_0) & \tilde{f}_1^{\lambda_1}(z_0) & \cdots & \tilde{f}_1^{\lambda_{2M-1}}(z_0) \\ \vdots & \vdots & & \vdots \\ \tilde{f}_1^{\lambda_0}(z_{M-1}) & \tilde{f}_1^{\lambda_1}(z_{M-1}) & \cdots & \tilde{f}_1^{\lambda_{2M-1}}(z_{M-1}) \end{bmatrix} \begin{bmatrix} C_0 \\ C_1 \\ \vdots \\ C_{2M-1} \end{bmatrix}. \tag{24}$$

This is a finite dimensional system of linear equations with $2M$ variables, which can be solved either analytically or numerically (the analytical expression can be obtained using Cramer's rule). However, the traditional numerical methods are not suitable for solving these equations since the coefficient matrix in Eq. (24) is too singular. Numerical computations indicate that traditional methods behave poorly when $M \geq 20$. To overcome this difficulty, note that the solution $\mathbf{x}$ to the linear equations $A\mathbf{x} = \mathbf{b}$ is also the solution to the optimization problem,

$$\min_{\mathbf{x}} \|A\mathbf{x} - \mathbf{b}\|^2.$$

Following this idea, we transform Eq. (24) into the following equivalent optimization problem:

$$\min_{C_n} \sum_{m=0}^{M} \left[\left| f_0(0,z_m) - \sum_{n=0}^{2M-1} C_n \tilde{f}_0^{\lambda_n}(z_m) \right|^2 + \left| f_1(0,z_m) - \sum_{n=0}^{2M-1} C_n \tilde{f}_1^{\lambda_n}(z_m) \right|^2 \right], \tag{25}$$

and then, we use the MATLAB function "quadprog" to solve it. Thus far, we have obtained the full time-dependent solution for the

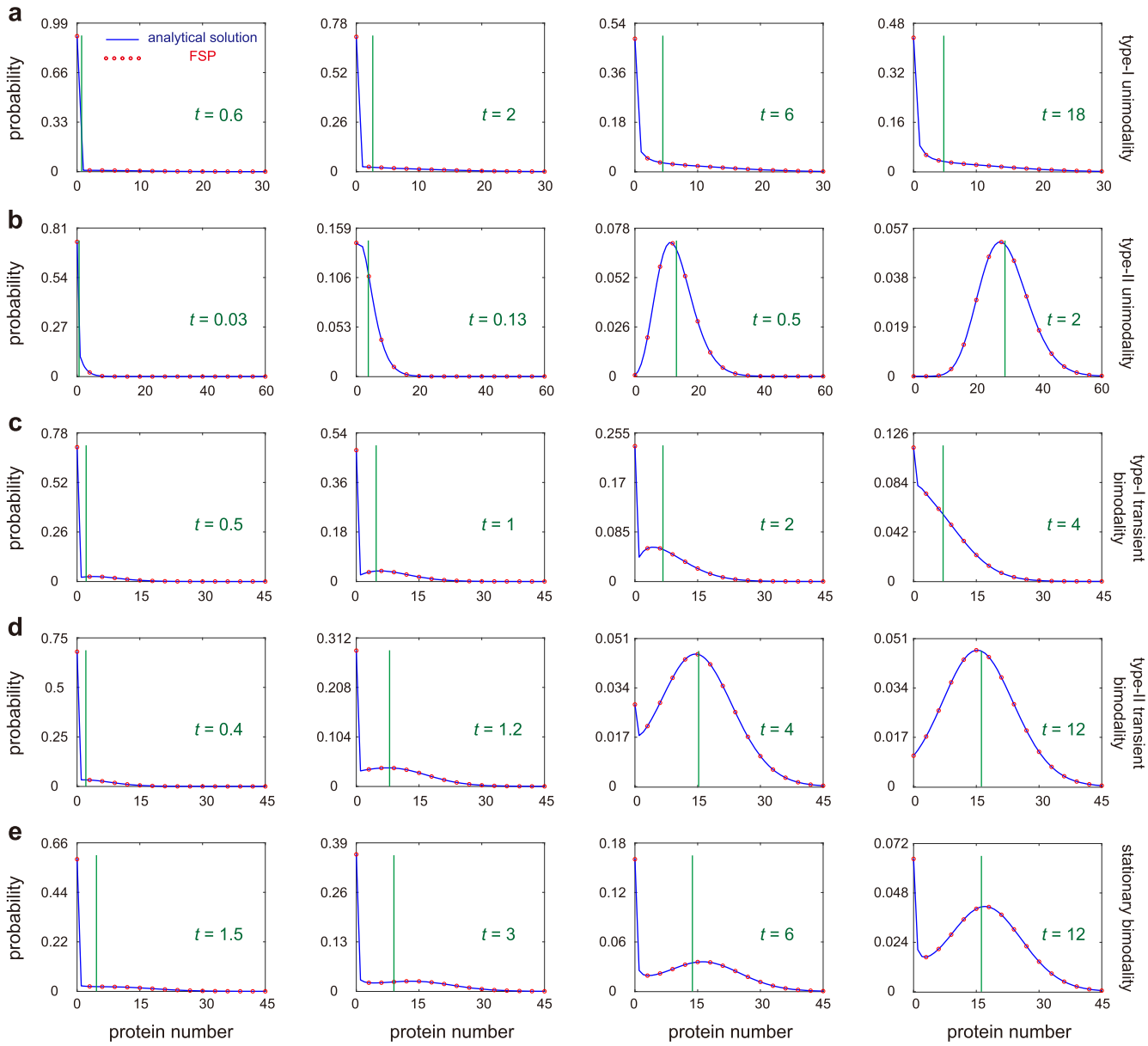

FIG. 2. Comparison of the semi-analytical and numerical solutions for five different types of dynamic behavior at four time points. The blue curves show the semi-analytical distributions given in Eqs. (22) and (23), the red circles show the numerical ones obtained from FSP, and the green vertical lines show the mean protein numbers. In the semi-analytical solution, the eigenvalues λ_n are computed by solving Eq. (17) (the number of layers of the continued fraction equation is truncated at $N = 200$) and the coefficient C_n are computed by solving Eq. (25) for $M = 50$. Here, we assume that initially the protein number is zero and the gene is off. (a) and (b) Unimodality. The distribution is unimodal at all times. (a) Type-I unimodality. The distribution peaks at zero at all times. The parameters are chosen as $\rho = 35$, $d = 1$, $\mu = 0.1$, $\nu = 0.2$, $a = 0.2$, $b = 1$, and $B = 1$. (b) Type-II unimodality. The distribution has a zero peak at small times and has a nonzero peak at large times. The parameters are chosen as $\rho = 35$, $d = 1$, $\mu = 0.5$, $\nu = 0.1$, $a = 80$, $b = 1$, and $B = 1$. (c) and (d) Transient bimodality. The distribution is unimodal at small and large times and is bimodal at intermediate times. (c) Type-I transient bimodality. The distribution has a zero peak at large times. The parameters are chosen as $\rho = 35$, $d = 1$, $\mu = 0$, $\nu = 0.3$, $a = 0.8$, $b = 0.1$, and $B = 1$. (d) Type-II transient bimodality. The distribution has a nonzero peak at large times. The parameters are chosen as $\rho = 35$, $d = 1$, $\mu = 0.2$, $\nu = 0.2$, $a = 1.2$, $b = 1$, and $B = 1$. (e) Stationary bimodality. The distribution is unimodal at small times and is bimodal at large times. The parameters are chosen as $\rho = 35$, $d = 1$, $\mu = 0.3$, $\nu = 0.2$, $a = 0.4$, $b = 1$, and $B = 1$.

bursty model. Note that when computing the eigenvalues λ_n and the coefficients C_n, there are numerical steps involved, and hence, our solution is only semi-analytical. In the special case where the gene is unregulated ($\mu = \nu = 0$), both the eigenvalues and coefficients can be computed exactly, allowing us to obtain a full analytical expression of the time-dependent distribution (see the Appendix).

To test our semi-analytical solution, we compare it with the numerical one obtained from the finite state projection algorithm (FSP).[29] The results are shown in Fig. 2. When using FSP, we truncate the state space at a large protein number N and solve the truncated master equation numerically using the MATLAB function "ODE45." The truncation size is chosen as $N = 5\rho B/d$. Since $\rho B/d$ is the typical protein number in the active gene state, the probability that the protein number is outside this truncation size is very small and practically can always be ignored. As expected, the two solutions agree perfectly at all times. According to our simulations, for most sets of model parameters, the semi-analytical solution is computationally faster than FSP when the mean protein number is larger than ~500; this is because the protein number needs to be truncated in FSP but does not in our solution.

B. Convergence to the steady-state solution

We next focus on the steady-state solution for the bursty model, which can be recovered from the time-dependent solution by taking $t \to \infty$. We have seen that when the system is ergodic, one eigenvalue is $\lambda_0 = 0$ and the other eigenvalues λ_n, $n \geq 1$, have negative real parts. Hence, the only term in Eq. (22) independent of time t is the first term, and all other terms tend to zero exponentially fast as $t \to \infty$. Then, the steady-state generating function is given by

$$f(t \to \infty, z) = \frac{\tilde{f}^{\lambda_0}(z)}{\tilde{f}^{\lambda_0}(1)} = \frac{{}_2F_1(a_1, b_1; c_1; w(z - z_0))}{{}_2F_1(a_1, b_1; c_1; w(1 - z_0))}, \tag{26}$$

where we have used the fact that $f(t, 1) = 1$. Taking the derivatives of the generating function f at $z = 0$ yields the steady-state protein distribution,

$$p_n(t \to \infty) = \frac{w^n (a_1)_n (b_1)_n}{n!(c_1)_n} \frac{{}_2F_1(a_1 + n, b_1 + n; c_1 + n; -wz_0)}{{}_2F_1(a_1, b_1; c_1; w(1 - z_0))}, \tag{27}$$

where $(a)_n = a(a + 1)\cdots(a + n - 1)$ denotes the Pochhammer symbol. Note that this is exactly the steady-state solution obtained previously in Ref. 22, which is a generalization of the special case of pure autoregulatory feedback studied earlier in Ref. 11.

C. Time-dependent solution for the non-bursty model

Next, we focus on the time-dependent protein distributions for the non-bursty model. In this case, the generating functions f_i and f still have the form of

$$f_i(t, z) = \sum_{n=0}^{\infty} C_n e^{\lambda_n t} \tilde{f}_i^{\lambda_n}(z), \qquad f(t, z) = \sum_{n=0}^{\infty} C_n e^{\lambda_n t} \tilde{f}^{\lambda_n}(z).$$

Recall that the non-bursty model given in Eq. (3) is a limiting case of the bursty model given in Eq. (1) when $\rho \to \infty$ and $B \to 0$ while keeping $\rho B = s$ as constant. In this limit, for the zero eigenvalue $\lambda_0 = 0$, the corresponding eigenfunction reduces to [Ref. 24, Eq. (13.18.2)]

$$\tilde{f}^{\lambda_0}(z) = {}_2F_1(a_1, b_1, c_1; w(z - z_0)) \to {}_1F_1(a_2; c_2; w'(z - z_0)),$$

where ${}_1F_1(a; c; z)$ is Kummer's confluent hypergeometric function and

$$a_2 = \frac{a}{\mu + d}, \quad c_2 = \frac{a + b}{\mu + \nu + d} + \frac{s\nu}{(\mu + \nu + d)^2}, \quad w' = \frac{s(\mu + d)}{d(\mu + \nu + d)}.$$

Moreover, in this limit, the Heun function Hf has the following limit (see Sec. 3 of the supplementary material for the proof):

$$Hf(\xi, q_1; \alpha_1, \beta_1, \gamma, 2 - \delta; x) \to Hc(q_3, \alpha_3, \gamma_3, \delta_3, \epsilon_3; x),$$

where Hc is the confluent Heun function[30] and

$$q_3 = -\frac{(\lambda + d)(a + b + \lambda)}{d(\mu + \nu + d)} - \frac{[(\mu + \nu)(a + \lambda) + d\nu]s}{d(\mu + \nu + d)^2},$$
$$\alpha_3 = -\frac{(\mu + a + d + \lambda)(\mu + \nu)s}{d(\mu + \nu + d)^2}, \quad \gamma_3 = \frac{a + b + \lambda}{\mu + \nu + d} + \frac{s\nu}{(\mu + \nu + d)^2},$$
$$\delta_3 = 2 + \frac{\lambda}{d}, \quad \epsilon_3 = -\frac{(\mu + \nu)(\mu + d)s}{d(\mu + \nu + d)^2}.$$

In addition, the continued fraction equation given in Eq. (17) reduces to

$$q_3 = \frac{R_0^{(3)} P_1^{(3)}}{(Q_1^{(3)} + q_3) -} \frac{R_1^{(3)} P_2^{(3)}}{(Q_2^{(3)} + q_3) -} \frac{R_2^{(3)} P_3^{(3)}}{(Q_3^{(3)} + q_3) -} \cdots, \tag{28}$$

where

$$R_n^{(3)} = -(n + 1)(n + \gamma_3), \quad P_n^{(3)} = \alpha_3 + (n - 1)\epsilon_3,$$
$$Q_n^{(3)} = n[-(n - 1 + \gamma_3) - \delta_3 + \epsilon_3].$$

Similar to the bursty case, all nonzero eigenvalues λ_n, $n \geq 1$, can be obtained by solving Eq. (28), and the corresponding eigenfunctions reduce to

$$\tilde{f}^{\lambda_n}(z) = (z - 1)Hf\left(\xi, q_1; \alpha_1, \beta_1, \gamma, 2 - \delta; \frac{\mu + \nu + d}{\mu + \nu}(z - z_0)\right)$$
$$\to (z - 1)Hc\left(q_3, \alpha_3, \gamma_3, \delta_3, \epsilon_3, \frac{\mu + \nu + d}{\mu + \nu}(z - z_0)\right), \quad n \geq 1.$$

So far, we have obtained all the eigenvalues λ_n and eigenfunctions $\tilde{f}^{\lambda_n}$. Similarly, by solving the optimization problem given in Eq. (25), we can compute all the coefficients C_n. This gives the complete time-dependent solution for the non-bursty model.

We emphasize that for the non-bursty model, the time-dependent solution has been discussed in Ref. 13 in the special case of negative feedback loops ($\mu = b = 0$). However, the solution derived in that paper is questionable due to the following two reasons. First, the authors did not show how to compute all the coef-

TABLE II. Comparison of the correct and incorrect eigenvalues in a negative autoregulatory loop. The first two rows show the true eigenvalues (first eight nonzero eigenvalues), and the third row shows the false eigenvalues computed using Eq. (29). The true eigenvalues are computed using both the continued fraction method (CFM) and the generator matrix method (GMM). Specifically, the first row shows the eigenvalues obtained by solving Eq. (28), and the second row shows the eigenvalues the generator matrix for the Markovian dynamics illustrated in Fig. 1(d). The parameters are chosen as $s = 20$, $d = 1$, $\nu = 0.1$, $a = 4$, and $\mu = b = 0$.

Eigenvalues	λ_1	λ_2	λ_3	λ_4	λ_5	λ_6	λ_7	λ_8
Correct (CFM)	−1.36	−2.97	$-4.05 + 0.81\mathbf{i}$	$-4.05 - 0.81\mathbf{i}$	$-5.10 + 1.13\mathbf{i}$	$-5.10 - 1.13\mathbf{i}$	$-6.15 + 1.37\mathbf{i}$	$-6.15 - 1.37\mathbf{i}$
Correct (GMM)	−1.36	−2.97	$-4.05 + 0.81\mathbf{i}$	$-4.05 - 0.81\mathbf{i}$	$-5.10 + 1.13\mathbf{i}$	$-5.10 - 1.13\mathbf{i}$	$-6.15 + 1.37\mathbf{i}$	$-6.15 - 1.37\mathbf{i}$
Incorrect	−1	−2	−3	−4	−5	−5.82	−6	−6.92

ficients C_n based on the initial conditions. Second, the eigenvalues computed in Ref. 13 are incorrect. The authors claimed that the system has two families of eigenvalues (these eigenvalues were first reported in an earlier paper[31] by the same authors),

$$\lambda_{1n} = -nd, \quad \lambda_{2n} = -(n+k)(d+\nu), \quad n \geq 0, \tag{29}$$

where $k = a/(d+\nu) + s\nu/(d+\nu)^2$. However, the correct eigenvalues should be all the solutions to the continued fraction equation. Table II compares the correct eigenvalues obtained by using the continued fraction and generator matrix methods and the incorrect eigenvalues given in Eq. (29). We observe significant deviations between them; the former can be complex numbers, while the latter are always real. In Sec. 4 of the supplementary material, we briefly explain how the false eigenvalues come from and further compare the true and false eigenvalues. Hence, the solution derived in Ref. 13 is both incomplete and incorrect. In the present paper, we addressed the above two points.

IV. DYNAMICAL PHASE DIAGRAMS

We next investigate the shape of the time-dependent distribution for the bursty model. In what follows, we assume that the initial protein number is zero and the gene is initially in the inactive state.[2] This mimics the situation where the gene has been silenced by some repressor over a period of time such that all protein molecules have been removed via degradation. At time $t = 0$, the repressor is removed, and we study how gene expression recovers. Under this initial condition, it is easy to see that $f_0(0,z) = 1$ and $f_1(0,z) = 0$.

In experiments, there are three commonly observed patterns for the protein distribution: a unimodal distribution with a zero peak (decaying distribution), a unimodal distribution with a nonzero peak (bell-shaped distribution), and a bimodal distribution with both a zero and a nonzero peak.[32,33] Our model is capable of producing all these three distribution patterns (Fig. 2). Among the three patterns, the bimodal one attracts the most attention since it separates isogenic cells into two distinct phenotypes.[34–36] To further understand the shape of the time-dependent protein distribution, we classify the dynamic behavior of our model into five different phases: (i) the distribution is decaying at all times [Fig. 2(a)], (ii) the distribution is decaying at small times and is bell-shaped at large times [Fig. 2(b)], (iii) the distribution is decaying at small and large times and is bimodal at intermediate times [Fig. 2(c)], (iv) the distribution is decaying at small times, is bimodal at intermediate times, and is bell-shaped at large times [Fig. 2(d)], and (v) the distribution is unimodal at small times and is bimodal at large times [Fig. 2(e)]. To distinguish between them, we refer to (i) as type-I of unimodality (U1), to (ii) as type-II of unimodality (U2), to (iii) as type-I of transient bimodality (TB1), to (iv) as type-II of transient bimodality, and to (v) as stationary bimodality (SB). The semi-analytical solution and numerical solution obtained from FSP indicate that all the five dynamical phases can appear when model parameters are appropriately chosen (Fig. 2).

To determine the regions for the five phases in the parameter space, we illustrate the a–b phase diagrams of our model in Figs. 3 and 4. In all phase diagrams, there is a unique point separating the five phases; this is analogous to the triple point in physics and chemistry where all three phases (gas, liquid, and solid) of a substance coexist in thermodynamic equilibrium.[37] Intriguingly, we find that the regions for TB1 and TB2 are often not adjacent in the phase diagram and are separated by the SB region (see, e.g., the middle row of Fig. 4). This is why we distinguish type-I from type-II transient bimodality in the present paper. Figure 3 shows the phase diagrams under different gene switching rates (slow switching, intermediate fast switching, and fast switching) and different feedback controls (positive feedback, coupled feedback, and negative feedback). We find that a positive feedback network fails to produce TB1, while a negative or coupled feedback network can produce all the five types of dynamical behavior. The region for transient and stationary bimodality (TB1, TB2, and SB) shrinks significantly as the switching rates increase. When the switching rates are relatively fast, the region for SB totally disappears in negative feedback networks, which agrees with the results found in Refs. 12 and 38, and the region for TB1 also disappears in all three types of networks. This indicates that TB1 can only appear when the switching rates are relatively slow. In particular, in the regime of relatively slow switching, positive feedback promotes the occurrence of SB and restrains the occurrence of TB1, while negative feedback promotes the occurrence of TB1 and restrains the occurrence of SB.

We next focus on Fig. 4, which illustrates the phase diagrams under different protein burst sizes and feedback controls when the switching rates are not too small. Again, TB1 is not found in the positive feedback case and SB is not found in the negative feedback case (note that SB can be found when gene switching is very slow, as previously shown in Fig. 3). From the phase diagram, as the burst size B increases, the region for SB shrinks in positive and coupled feedback networks; the region for TB2 enlarges significantly in all three types of networks; the region for TB1 remains almost unchanged in negative feedback networks, while the region for SB

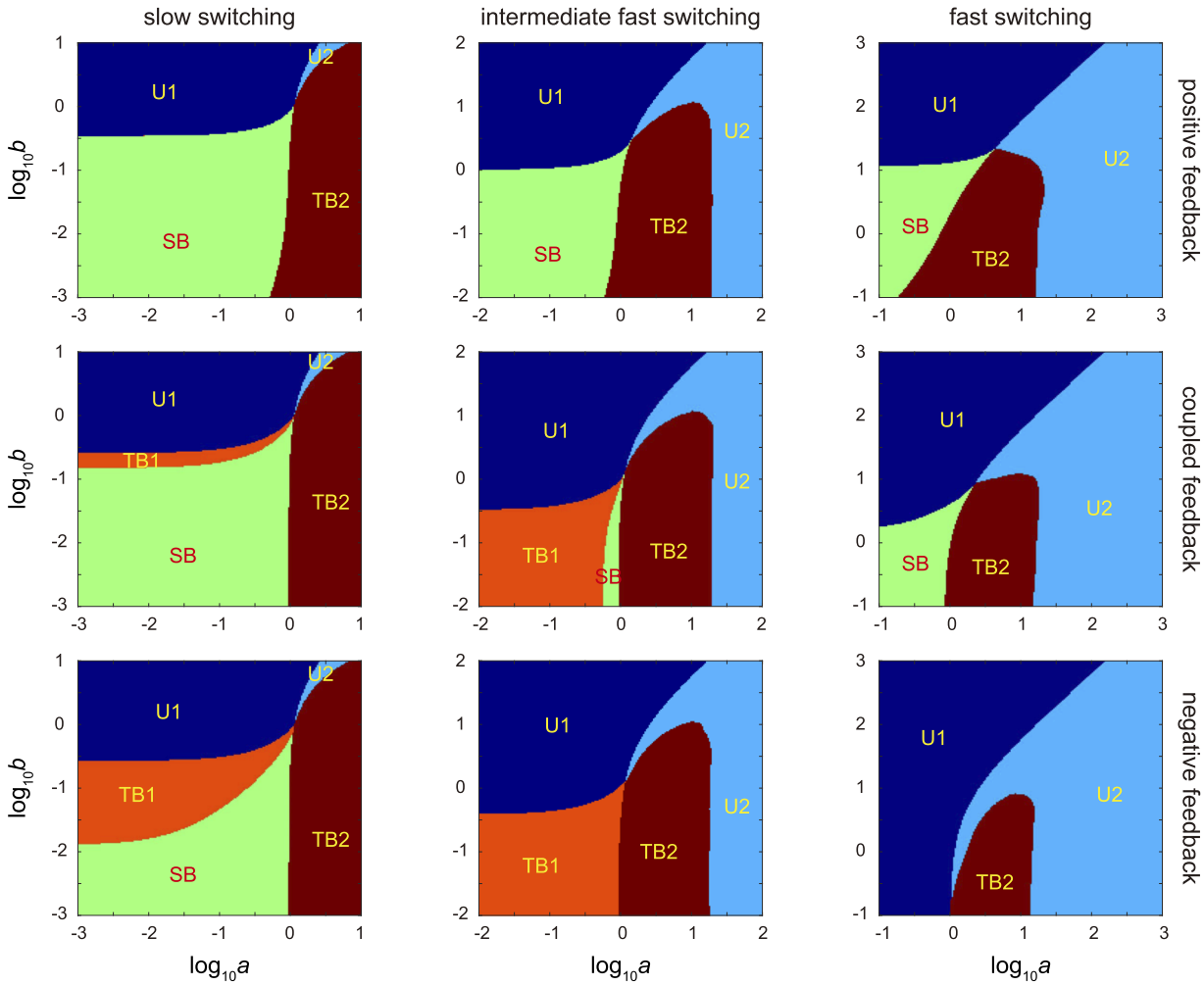

FIG. 3. Dynamical phase diagrams in the a–b plane (here, a and b are the spontaneous switching rates between the two gene states) under different switching rates and feedback controls. The system can produce five different types of dynamical behavior: type-I unimodality (U1, dark blue), type-II unimodality (U2, light blue), type-I transient bimodality (TB1, orange), type-II transient bimodality (TB2, brown), and stationary bimodality (SB, green). Note that in our model, the gene switching rates are $a + \mu n$ and $b + \nu n$, with μ and ν being the strengths of positive and negative feedback loops, respectively. In slow switching conditions, the ranges of a and b are chosen to be 10^{-3}–10^{1}, and the feedback strengths are chosen as $\mu = 0.0225$, $\nu = 0$ for positive feedback, $\mu = 0.009$, $\nu = 0.015$ for coupled feedback, and $\mu = 0$, $\nu = 0.0225$ for negative feedback. In intermediate fast switching conditions, the ranges of a and b are chosen to be 10^{-2}–10^{2}, and the feedback strengths are chosen as $\mu = 0.225$, $\nu = 0$ for positive feedback, $\mu = 0.09$, $\nu = 0.15$ for coupled feedback, and $\mu = 0$, $\nu = 0.225$ for negative feedback. In fast switching conditions, the ranges of a and b are chosen to be 10^{-1}–10^{3}, and the feedback strengths are chosen as $\mu = 2.25$, $\nu = 0$ for positive feedback, $\mu = 0.9$, $\nu = 1.5$ for coupled feedback, and $\mu = 0$, $\nu = 2.25$ for negative feedback. The other parameters are chosen as $d = 1$, $B = 1$, $\rho = 15$.

converts to that for TB1 in coupled feedback networks. In summary, we find that TB1 is mostly likely to occur in negative and coupled feedback networks when gene switching is not too fast; TB2 is mostly affected by the burst size; and SB is sensitive to many factors and is mostly likely to occur in positive and coupled feedback networks when gene switching is relatively slow and the burst size is small.

Among the five dynamical phases, TB1 is of particular interest because it can never occur when the gene is unregulated ($\mu = \nu = 0$). In fact, for the two-state telegraph model of stochastic gene expression, it has been shown that it can produce U1, U2, TB2, and SB but fails to produce TB1.[39,40] In fact, TB1 has been observed recently in single-cell experiments [see Fig. 2(c) in Ref. 41]. Previous studies have used a four-state gene expression model to fit the data but the model does not involve feedback.[41] Our results show that the presence of negative or coupled feedback loops is possibly another important origin for the experimentally observed TB1 dynamics.

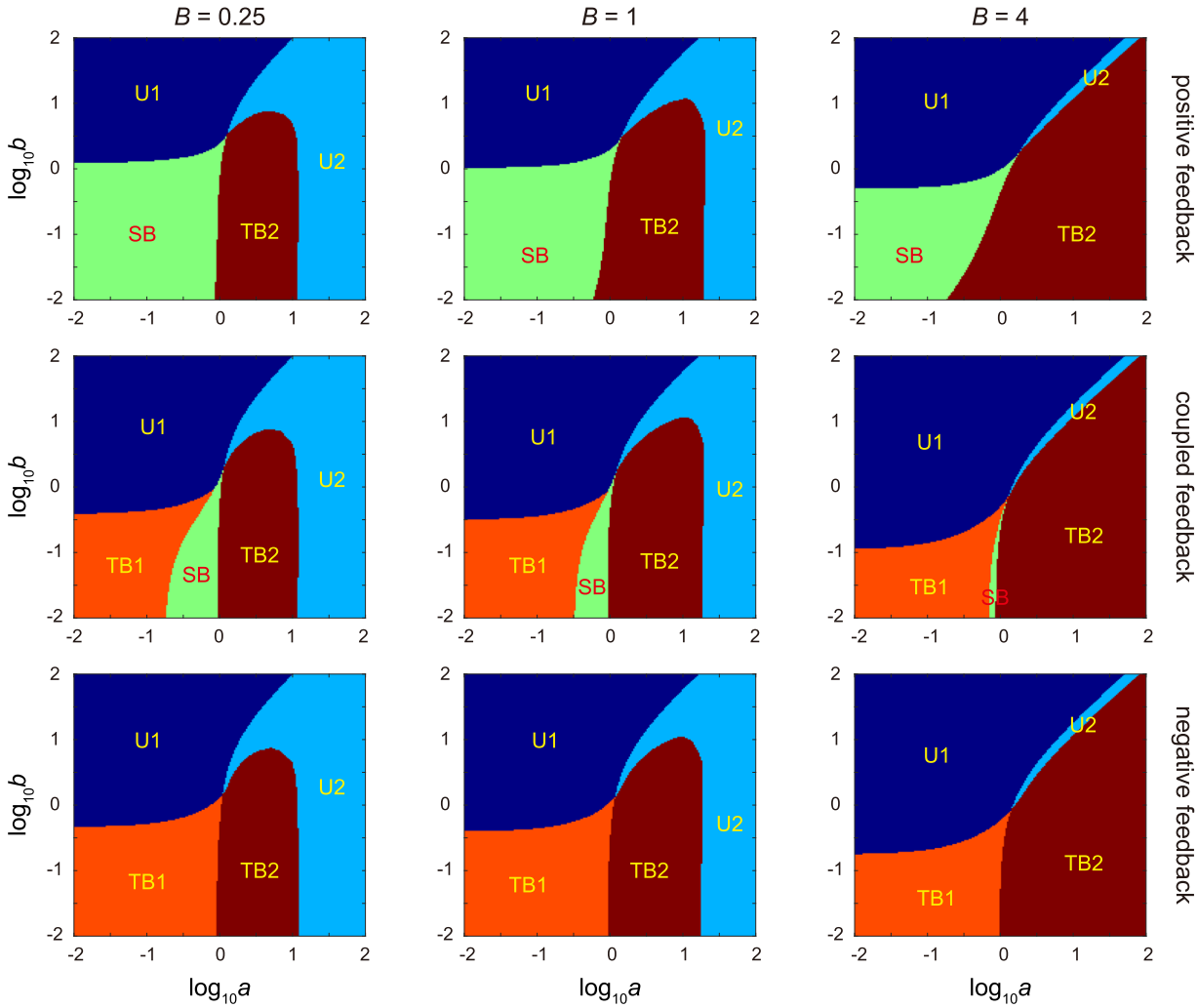

FIG. 4. Dynamical phase diagrams in the a–b plane (here, a and b are the spontaneous switching rates between the two gene states) under different burst sizes and feedback controls. The system can produce five different types of dynamical behavior: U1 (dark blue), U2 (light blue), TB1 (orange), TB2 (brown), and SB (green). The protein burst size is chosen as $B = 0.25$ (left), $B = 1$ (middle), and $B = 4$ (right). The feedback strengths are chosen as $\mu = 0.2$, $\nu = 0$ for positive feedback (upper), $\mu = \nu = 0.1$ for coupled feedback (middle), and $\mu = 0$, $\nu = 0.2$ for negative feedback (below). The other parameters are chosen as $d = 1$ and ρ is tuned so that the typical protein number $\rho B/d = 15$ in the active gene state remains invariant.

V. CONCLUSION

In this work, we semi-analytically solved the CMEs and obtained the full time-dependence of a minimal coupled positive-plus-negative feedback loop with gene state switching, protein synthesis, and protein decay. This coupled gene circuit includes positive and negative autoregulatory feedback loops as special cases. In the active gene state, our model assumes that the protein is produced in a non-bursty or bursty manner. Following previous work,[42] we transformed the CMEs satisfied by the protein distribution into the PDEs satisfied by the generating function. By using the method of spectral decomposition, we represented the protein distribution as a weighted sum of eigenvalue terms, which only depends on time, and eigenfunction terms, which only depends on the spatial variable. We then make nontrivial spatial and functional transformations to obtain a Heun differential equation satisfied by the eigenfunctions.

Interestingly, the eigenfunctions are all local Heun functions, while the eigenvalues are those values such that these functions are holomorphic on the unit disk and can be determined by solving a continued fraction equation. In general, these eigenvalues cannot be computed in closed form. However, in the special case where the gene is unregulated, the eigenvalues can be solved exactly and the eigenfunctions reduce to Gaussian hypergeometric functions. We finally use a method similar to the inverse discrete Fourier transform to compute the weights of these eigenvalue and eigenfunction terms based on the initial conditions. In particular, our

TABLE III. Comparison of properties for self-adjoint operators, normal operators, and the operator studied in this paper.

Type of operators	Eigenvalues	Eigenfunctions
Self-adjoint operators	Real	Orthogonal
Normal operators	Complex	Orthogonal
Differential operator in Eq. (6)	Complex	Non-orthogonal

time-dependent solution generalizes the one obtained in Ref. 38, which can be applied only in fast switching conditions, and also generalizes and modifies the incomplete and incorrect solution obtained in Ref. 13 for the non-bursty case. The eigenvalues obtained in Ref. 13 are incorrect since they are all real, while the true eigenvalues can be complex numbers. The complex eigenvalues may be related to the oscillatory[43,44] and adaptation[45,46] phenomena observed in negative feedback networks. Finally, we investigated the dynamical phase diagram of the coupled feedback loop by categorizing regions of parameter space according to five distinct types of time-evolution. This allowed us to deduce relationships between these phases and the type of feedback loop (positive, coupled, and negative), the burst size, and the speed of gene switching.

Our analytical theory also has mathematical importance. In the classical functional analysis textbooks,[47] spectral decomposition for unbounded operators is only well developed when the operator is self-adjoint or normal. For a self-adjoint operator, the eigenvalues are all real and the eigenfunctions are orthogonal. In this case, the eigenvalues and eigenfunctions can sometimes be determined analytically[48,49] using, e.g., the Sturm–Liouville theory. However, the unbounded operator studied in this paper, i.e., the differential operator in Eq. (6), is neither self-adjoint nor normal (see Table III for the comparison between the three types of operators). For this operator, the eigenvalues can be complex and the eigenfunctions are non-orthogonal. While we have showed that the eigenfunctions satisfy an second-order differential equation [see Eq. (10)], this equation cannot be transformed into a classical Strum–Liouville problem, and thus, the conventional method fails. Here, we obtain the complete spectral decomposition for a special non-self-adjoint and non-normal operator. We anticipate that a new spectral theory could be developed for general non-self-adjoint and non-normal operators in the near future.

Our model has two notable limitations: (i) We assume that there is no change in the protein number during gene activation and inactivation. However, in reality, the protein number decreases by one when a protein copy binds to a gene and increases by one when unbinding occurs.[10,12] In other words, the present model ignores the protein–gene binding fluctuations, and hence, it may not be accurate when the protein number is very small or when the feedback strength is very strong.[12,50] The reason why we make this approximation is that if we ignore the binding fluctuations, then the differential equation satisfied by the eigenfunctions has four regular singularities and, thus, can be transformed into a Heun differential equation. However, if we take the binding fluctuations into account, then the differential equation will have five regular singularities and, thus, does not allow an existing special function representation. (ii) The model does not have an explicit cell cycle description. In reality, most proteins are not continuously degraded at some positive rate, but rather because their half-lives are often much longer than the cell cycle duration itself,[17,51,52] they tend to accumulate during the cell cycle and then (approximately) half at cell division. Under some conditions, the modelling of protein degradation via a first-order reaction (as in our current model) well approximates the dilution due to cell division.[53] Note that our model with $d = 0$ can also be seen as predicting the time-dependent protein distribution within a cell cycle where $t = 0$ corresponds to the birth of a cell, but since there is no explicit modelling of cell division, it cannot predict how the distributions change from one generation to another. In the forthcoming part II of this work, we will address some of these issues.

SUPPLEMENTARY MATERIAL

The supplementary material contains detailed proofs and calculations of some key results in the main text.

ACKNOWLEDGMENTS

The authors thank Dr. Youming Li for stimulating discussion. J.H. acknowledges support from National Science Foundation Grant Nos. EF-2133863 and DMR-191073. R.G. acknowledges support from the Leverhulme Trust (Grant No. RPG-2020-327). C.J. acknowledges support from the National Natural Science Foundation of China with Grant Nos. U2230402 and 12271020.

AUTHOR DECLARATIONS

Conflict of Interest

The authors have no conflicts to disclose.

Author Contributions

Bingjie Wu: Formal analysis (equal); Investigation (equal); Writing – original draft (equal); Writing – review & editing (equal). **James Holehouse**: Formal analysis (equal); Investigation (equal); Writing – review & editing (equal). **Ramon Grima**: Conceptualization (equal); Funding acquisition (equal); Supervision (equal); Writing – review & editing (equal). **Chen Jia**: Conceptualization (equal); Formal analysis (equal); Funding acquisition (equal); Investigation (equal); Supervision (equal); Writing – original draft (equal); Writing – review & editing (equal).

DATA AVAILABILITY

Data sharing is not applicable to this article as no new data were created or analyzed in this study.

APPENDIX: TIME-DEPENDENT SOLUTION FOR UNREGULATED GENES

We focus on the time-dependent protein distributions for an unregulated gene. If a gene is unregulated, then

its expression dynamics can be described by the reaction scheme,

$$G \underset{b}{\overset{a}{\rightleftharpoons}} G^*, \quad G^* \xrightarrow{\rho p^k(1-p)} G^* + kP, \quad k \geq 1, \quad P \xrightarrow{d} \varnothing.$$

This is a special case of Eq. (1) when the positive and negative feedback strengths both vanish, i.e., $\mu = \nu = 0$. We emphasize that for an unregulated gene, the analytical time-dependent distributions of protein numbers have been derived in Refs. 54 and 55. Here, we will provide a different explicit expression of the time-dependent solution.

When $\mu = \nu = 0$, the expressions of the eigenvalues λ_n, eigenfunctions $\tilde{f}^{\lambda_n}$, and coefficients C_n in Eq. (22) can be simplified to a great extent. In this case, the related parameters in Eq. (18) reduce to

$$z_0 = 1, \quad w = B, \quad c_1 = \frac{a+b}{d}, \quad a_1 + b_1 = \frac{a+b+\rho}{d}, \quad a_1 b_1 = \frac{a\rho}{d^2}. \tag{A1}$$

It can be proved that the system has two families of eigenvalues (see Sec. 5 of the supplementary material for details),

$$\lambda_{1n} = -nd, \quad \lambda_{2n} = -(a+b+nd), \quad n \geq 0, \tag{A2}$$

which can be computed explicitly. For the family of eigenvalues $\lambda_{1n} = -nd$, the corresponding eigenfunctions are given by

$$\tilde{f}^{\lambda_{1n}}(z) = (z-1)^n y_1(z),$$

and for the other family of eigenvalues $\lambda_{2n} = -(a+b+nd)$, the corresponding eigenfunctions are given by

$$\tilde{f}^{\lambda_{2n}}(z) = (z-1)^{n+1} y_2(z),$$

where

$$y_1(z) = {}_2F_1(a_1, b_1; c_1; B(z-1)),$$
$$y_2(z) = {}_2F_1(a_1+1-c_1, b_1+1-c_1, 2-c_1; B(z-1)),$$

and a_1, b_1, and c_1 are given in Eq. (A1). Hence, for an unregulated gene, the generating function f has the form of

$$f(t,z) = \sum_{n=0}^{\infty} C_{1n} e^{-ndt} (z-1)^n y_1(z) + \sum_{n=0}^{\infty} C_{2n} e^{-(a+b+nd)t} (z-1)^{n+1} y_2(z).$$

Finally, we show how to determine the coefficients C_{1n} and C_{2n}. Let F_n^i be the unnormalized nth factorial moment of the protein number at time $t = 0$ when the gene is in state i, i.e.,

$$F_n^i = \sum_{m=0}^{\infty} m(m+1)\cdots(m+n-1) p_{i,m}(0) = \frac{\partial^n f_i}{\partial z^n}(0,z)\bigg|_{z=1}.$$

It is easy to see that $C_{10} = 1$, and the remaining coefficients can be computed inductively as follows (see Sec. 5 of the supplementary material for details):

$$\begin{aligned} C_{1n} &= \frac{F_n^0 + F_n^1 - \sum_{m=0}^{n-1} C_{1m} m! \zeta_{n-m} - \sum_{m=0}^{n-1} C_{2m}(m+1)! \xi_{n-m-1}}{n!}, \quad n \geq 1, \\ C_{2n} &= \frac{\sum_{m=0}^{n} C_{1m} m! \kappa_{n-m} - \sum_{m=0}^{n-1} C_{2m} m! \eta_{n-m} + \sum_{m=0}^{n-1} C_{2m}(m+1)! \theta_{n-m-1} - \rho p F_n^1}{(a+b-d)(1-p)n!}, \quad n \geq 0, \end{aligned} \tag{A3}$$

where

$$\zeta_n = \frac{B^n (a_1)_n (b_1)_n}{(c_1)_n}, \quad \xi_n = \frac{B^n (a_1+1-c_1)_n (b_1+1-c_1)_n}{(2-c_1)_n},$$
$$\kappa_n = (1-p)\zeta_{n+1} - np\zeta_n, \quad \eta_n = (a+b-d)[(1-p)\xi_n - np\xi_{n-1}],$$
$$\theta_n = d[(1-p)\xi_{n+1} - np\xi_n].$$

Now, we focus on the initial condition in Sec. IV, i.e., initially the protein number is zero and the gene is inactive. In this case, we have $f_0(0,z) = 1$ and $f_1(0,z) = 0$. This clearly shows that $F_0^0 = 1$ and $F_n^0 = 0$ for all $n \geq 1$ and $F_n^1 = 0$ for all $n \geq 0$. Inserting these values of F_n^i into Eq. (A3) gives the values of all the coefficients C_{1n} and C_{2n}.

REFERENCES

[1] E. H. Davidson, *The Regulatory Genome: Gene Regulatory Networks in Development and Evolution* (Elsevier, 2010).

[2] N. Rosenfeld, M. B. Elowitz, and U. Alon, "Negative autoregulation speeds the response times of transcription networks," J. Mol. Biol. **323**, 785–793 (2002).

[3] S. S. Shen-Orr, R. Milo, S. Mangan, and U. Alon, "Network motifs in the transcriptional regulation network of *Escherichia coli*," Nat. Genet. **31**, 64–68 (2002).

[4] N. Friedman, L. Cai, and X. S. Xie, "Linking stochastic dynamics to population distribution: An analytical framework of gene expression," Phys. Rev. Lett. **97**, 168302 (2006).

[5] M. C. Mackey, M. Tyran-Kaminska, and R. Yvinec, "Dynamic behavior of stochastic gene expression models in the presence of bursting," SIAM J. Appl. Math. **73**, 1830–1852 (2013).

[6] P. Bokes and A. Singh, "Protein copy number distributions for a self-regulating gene in the presence of decoy binding sites," PLoS One **10**, e0120555 (2015).

[7] M. Pájaro, A. A. Alonso, and C. Vázquez, "Shaping protein distributions in stochastic self-regulated gene expression networks," Phys. Rev. E **92**, 032712 (2015).

[8] C. Jia, M. Q. Zhang, and H. Qian, "Emergent Lévy behavior in single-cell stochastic gene expression," Phys. Rev. E **96**, 040402(R) (2017).

[9] J. E. Hornos *et al.*, "Self-regulating gene: An exact solution," Phys. Rev. E **72**, 051907 (2005).

[10] R. Grima, D. R. Schmidt, and T. J. Newman, "Steady-state fluctuations of a genetic feedback loop: An exact solution," J. Chem. Phys. **137**, 035104 (2012).

[11]N. Kumar, T. Platini, and R. V. Kulkarni, "Exact distributions for stochastic gene expression models with bursting and feedback," Phys. Rev. Lett. **113**, 268105 (2014).
[12]C. Jia and R. Grima, "Small protein number effects in stochastic models of autoregulated bursty gene expression," J. Chem. Phys. **152**, 084115 (2020).
[13]A. F. Ramos, G. C. Innocentini, and J. E. M. Hornos, "Exact time-dependent solutions for a self-regulating gene," Phys. Rev. E **83**, 062902 (2011).
[14]J. Holehouse, Z. Cao, and R. Grima, "Stochastic modeling of autoregulatory genetic feedback loops: A review and comparative study," Biophys. J. **118**, 1517–1525 (2020).
[15]J. Paulsson, "Models of stochastic gene expression," Phys. Life Rev. **2**, 157–175 (2005).
[16]C. Jia, "Simplification of Markov chains with infinite state space and the mathematical theory of random gene expression bursts," Phys. Rev. E **96**, 032402 (2017).
[17]B. Schwanhäusser *et al.*, "Global quantification of mammalian gene expression control," Nature **473**, 337 (2011).
[18]J. Paulsson and M. Ehrenberg, "Noise in a minimal regulatory network: Plasmid copy number control," Q. Rev. Biophys. **34**, 1–59 (2001).
[19]L. Cai, N. Friedman, and X. S. Xie, "Stochastic protein expression in individual cells at the single molecule level," Nature **440**, 358–362 (2006).
[20]T. Y.-C. Tsai *et al.*, "Robust, tunable biological oscillations from interlinked positive and negative feedback loops," Science **321**, 126–129 (2008).
[21]P. Liu, Z. Yuan, H. Wang, and T. Zhou, "Decomposition and tunability of expression noise in the presence of coupled feedbacks," Chaos **26**, 043108 (2016).
[22]C. Jia, L. Y. Wang, G. G. Yin, and M. Q. Zhang, "Single-cell stochastic gene expression kinetics with coupled positive-plus-negative feedback," Phys. Rev. E **100**, 052406 (2019).
[23]C. Jia and Y. Li, "Analytical time-dependent distributions for gene expression models with complex promoter switching mechanisms," SIAM J. Appl. Math. **83**, 1572–1602 (2023).
[24]F. W. J. Olver *et al.*, NIST digital library of mathematical functions, http://dlmf.nist.gov/, release 1.0.17 of 2017-12-22.
[25]A. Ronveaux, *Heun's Differential Equations* (The Clarendon Press, Oxford University Press, New York, 1995).
[26]R. Maier, "The 192 solutions of the Heun equation," Math. Comput. **76**, 811–843 (2007).
[27]W. Rudin, *Principles of Mathematical Analysis* (McGraw Hill, 1953).
[28]J. Holehouse and J. Moran, "Exact time-dependent dynamics of discrete binary choice models," J. Phys.: Complexity **3**, 035005 (2022).
[29]B. Munsky and M. Khammash, "The finite state projection algorithm for the solution of the chemical master equation," J. Chem. Phys. **124**, 044104 (2006).
[30]O. V. Motygin, "On evaluation of the confluent Heun functions," in *2018 Days on Diffraction (DD)* (IEEE, 2018), Vol. 223–229.
[31]A. F. Ramos and J. E. Hornos, "Symmetry and stochastic gene regulation," Phys. Rev. Lett. **99**, 108103 (2007).
[32]B. Munsky, G. Neuert, and A. Van Oudenaarden, "Using gene expression noise to understand gene regulation," Science **336**, 183–187 (2012).
[33]F. Jiao, Q. Sun, M. Tang, J. Yu, and B. Zheng, "Distribution modes and their corresponding parameter regions in stochastic gene transcription," SIAM J. Appl. Math. **75**, 2396–2420 (2015).
[34]M. Kærn, T. C. Elston, W. J. Blake, and J. J. Collins, "Stochasticity in gene expression: From theories to phenotypes," Nat. Rev. Genet. **6**, 451–464 (2005).
[35]C. Jia, M. Qian, Y. Kang, and D. Jiang, "Modeling stochastic phenotype switching and bet-hedging in bacteria: Stochastic nonlinear dynamics and critical state identification," Quant. Biol. **2**, 110–125 (2014).
[36]P. Thomas, N. Popovic, and R. Grima, "Phenotypic switching in gene regulatory networks," Proc. Natl. Acad. Sci. U. S. A. **111**, 6994–6999 (2014).
[37]A. D. McNaught, A. Wilkinson *et al.*, *Compendium of Chemical Terminology* (Blackwell Science, Oxford, 1997), Vol. 1669.
[38]C. Jia and R. Grima, "Dynamical phase diagram of an auto-regulating gene in fast switching conditions," J. Chem. Phys. **152**, 174110 (2020).
[39]F. Jiao, M. Tang, and J. Yu, "Distribution profiles and their dynamic transition in stochastic gene transcription," J. Differ. Equations **254**, 3307–3328 (2013).
[40]F. Jiao, J. Ren, and J. Yu, "Analytical formula and dynamic profile of mRNA distribution," Discrete Contin. Dyn. Syst. B **25**, 241–257 (2019).
[41]G. Neuert *et al.*, "Systematic identification of signal-activated stochastic gene regulation," Science **339**, 584–587 (2013).
[42]O. G. Berg, "A model for the statistical fluctuations of protein numbers in a microbial population," J. Theor. Biol. **71**, 587–603 (1978).
[43]B. Novák and J. J. Tyson, "Design principles of biochemical oscillators," Nat. Rev. Mol. Cell Biol. **9**, 981–991 (2008).
[44]A. Gupta and M. Khammash, "Frequency spectra and the color of cellular noise," Nat. Commun. **13**, 4305 (2022).
[45]W. Ma, A. Trusina, H. El-Samad, W. A. Lim, and C. Tang, "Defining network topologies that can achieve biochemical adaptation," Cell **138**, 760–773 (2009).
[46]C. Jia and M. Qian, "Nonequilibrium enhances adaptation efficiency of stochastic biochemical systems," PLoS One **11**, e0155838 (2016).
[47]W. Rudin, *Functional Analysis*, 2nd ed., *International Series in Pure and Applied Mathematics* (McGraw-Hill, New York, 1991).
[48]M. Assaf and B. Meerson, "Spectral theory of metastability and extinction in birth-death systems," Phys. Rev. Lett. **97**, 200602 (2006).
[49]C. Jia, H. Qian, M. Chen, and M. Q. Zhang, "Relaxation rates of gene expression kinetics reveal the feedback signs of autoregulatory gene networks," J. Chem. Phys. **148**, 095102 (2018).
[50]J. Holehouse and R. Grima, "Revisiting the reduction of stochastic models of genetic feedback loops with fast promoter switching," Biophys. J. **117**, 1311–1330 (2019).
[51]R. Christiano, N. Nagaraj, F. Fröhlich, and T. C. Walther, "Global proteome turnover analyses of the yeasts *S. cerevisiae* and *S. pombe*," Cell Rep. **9**, 1959–1965 (2014).
[52]C. Jia and R. Grima, "Frequency domain analysis of fluctuations of mRNA and protein copy numbers within a cell lineage: Theory and experimental validation," Phys. Rev. X **11**, 021032 (2021).
[53]C. H. Beentjes, R. Perez-Carrasco, and R. Grima, "Exact solution of stochastic gene expression models with bursting, cell cycle and replication dynamics," Phys. Rev. E **101**, 032403 (2020).
[54]S. Iyer-Biswas, F. Hayot, and C. Jayaprakash, "Stochasticity of gene products from transcriptional pulsing," Phys. Rev. E **79**, 031911 (2009).
[55]Z. Cao and R. Grima, "Linear mapping approximation of gene regulatory networks with stochastic dynamics," Nat. Commun. **9**, 3305 (2018).